Tuning properties of radial phantom motion aftereffects

Nicholas S.C. Price *, John A. Greenwood, Michael R. Ibbotson

Department of Visual Sciences, Research School of Biological Sciences, Australian National University, Box 475 Canberra ACT 2601, Australia

Abstract

Motion aftereffects are normally tested in regions of the visual field that have been directly exposed to motion (*local* or *concrete* MAEs). We compared *concrete* MAEs with *remote* or *phantom* MAEs, in which motion is perceived in regions not previously adapted to motion. Our aim was to study the spatial dependencies and spatiotemporal tuning of phantom MAEs generated by radially expanding stimuli. For concrete and phantom MAEs, peripheral stimuli generated stronger aftereffects than central stimuli. Concrete MAEs display temporal frequency tuning, while phantom MAEs do not show categorical temporal frequency or velocity tuning. We found that subjects may use different response strategies to determine motion direction when presented with different stimulus sizes. In some subjects, as adapting stimulus size increased, phantom MAE strength increased while the concrete MAE strength decreased; in other subjects, the opposite effects were observed. We hypothesise that these opposing findings reflect interplay between the adaptation of global motion sensors and local motion sensors with inhibitory interconnections.
© 2004 Elsevier Ltd. All rights reserved.

Keywords: Motion aftereffect; Adaptation; Temporal frequency; *Phantom*

1. Introduction

Cortical processing of visual motion is performed by a hierarchy of brain areas. At the lowest level, area V1 contains motion detectors sensitive to translation in small regions of the visual field (classical receptive field diameter <2°) (Cavanaugh, Bair, & Movshon, 2002). Processing of translation by area MT has a more global focus, because the receptive field sizes are larger, extending up to 20° in diameter (Tanaka et al., 1986). Area MST has global motion detectors with receptive fields up to 100° in diameter, sensitive to complex motions associated with optic flow generated by body and eye movements (Duffy & Wurtz, 1991). As the size of the visual field analysed by a single cell increases, there is an increase in the complexity of the motion that it is most sensitive to, from local translation to global translation, radiation or rotation.

Local and global motion detectors have been extensively studied using a psychophysical phenomenon, the motion aftereffect (MAE, for review, see Wade, 1994).

Following prolonged viewing of a moving scene, stationary texture appears to move in the opposite direction. The MAE can be produced by translational motion and by more complex motion. Thus after adaptation to an expanding figure, a static figure appears to contract. Typically, the MAEs produced by radial or rotational movements are stronger than those associated with translational motion (Bex, Metha, & Makous, 1999). This suggests that adaptation is occurring at multiple levels of motion processing, with the MAE the product of cumulative adaptation at several levels.

Further evidence for a hierarchy of motion processing comes from the "phantom" or "remote" MAE, in which aftereffects can be expressed in areas of the visual field unadapted by motion (Bex et al., 1999; Bonnet & Pouthas, 1972; Hershenson, 1984; Snowden & Milne, 1997; von Grunau & Dube, 1992; Wade & Salvano-Pardieu, 1998; Wade, Spillmann, & Swanston, 1996). The phantom MAE arises when motion is used to adapt one region of the visual field but the MAE is expressed in another location. The resulting MAE is weaker than the associated "concrete" or "local" MAE, in which the adaptation and test stimuli occupy the same region of the visual field. One important feature of the phantom

---

* Corresponding author.
E-mail address: nprice@rsbs.anu.edu.au (N.S.C. Price).

MAE is that no motion is perceived in the test region during adaptation. This distinguishes it from some reports of MAEs in unadapted locations, which may be attributed to illusory contours (von Grunau, 1986; Weisstein, Maguire, & Berbaum, 1977; Zaidi & Sachtler, 1991) or motion contrast (Nawrot & Sekuler, 1990). We do not regard the latter effects as true remote or phantom motion aftereffects because the perceived motion in the test region may play a role in directly adapting low-level, local motion processing pathways. This may occur in area 18, where cells can detect subjective contours (von der Heydt, Peterhans, & Baumgartner, 1984).

Snowden and Milne (1997) adapted subjects to radial, rotational or translational motion in two horizontal quadrants. MAEs were then tested in two vertical quadrants, giving phantom MAEs because the adapting and test stimuli did not overlap. Concrete MAEs were also assessed using test stimuli in the same horizontal quadrants as the adapting stimuli. It was found that rotation produced larger MAEs than translation, expansion or contraction, with phantom MAEs approximately half the size of concrete MAEs. A similar study using four Gabor patches arranged in non-overlapping '+' or 'X' configurations found similar results (Bex et al., 1999). Snowden and Milne also adapted subjects to translation characteristic of clockwise rotation by presenting upwards motion in the left quadrant and downwards motion in the right quadrant. When tested in the non-overlapping vertical quadrants, subjects perceived a counterclockwise phantom MAE. Thus the phantom MAE is not explicable simply in terms of poor fixation or areal spreading of a translational MAE (Bonnet & Pouthas, 1972), since the perceived MAE is orthogonal to the adapting stimulus.

While the existence of phantom MAEs has been conclusively demonstrated, the physiological basis of their generation remains unresolved. We address a number of issues relating to this.

(1) Firstly, recent physiological data suggests that neurons in area MT are velocity tuned across a wide range of spatial frequencies (Perrone & Thiele, 2001, 2002; Priebe, Cassanello, & Lisberger, 2003). In contrast, direction-selective cells earlier in the processing hierarchy are temporal frequency tuned (Foster, Gaska, Nagler, & Pollen, 1985). Therefore, it may be possible to infer the locus of the phantom MAE by studying whether it shows velocity or temporal frequency tuning.
(2) Secondly, we examine the influence of stimulus eccentricity. It is known that the MAE associated with small-field translation increases in strength as the adapting stimulus is moved from central to peripheral locations (Murakami & Shimojo, 1995; Wright, 1986). However, the effects of eccentricity

on MAEs produced by complex motion have not been studied.
(3) Finally, we consider the effects of varying the size of the adapting and test areas. It is likely that cells with large receptive fields, such as those in area MT or MST are responsible for producing phantom MAEs. This suggests that increasing the size of an adapting stimulus would increase the physiological responses of a cell and hence increase its level of adaptation and the corresponding MAE.

2. Methods

2.1. Stimuli

Stimuli were generated on a VSG2/5 graphics card (Cambridge Research Systems, Ltd.) and displayed at 100 Hz on a 20″ monitor (Eizo T662-T, 800 × 640 pixels). Concentric rings with sinusoidal luminance profile and 50% Michelson contrast were used as adapting stimuli (Fig. 1). Their spatial frequencies (SF: 1.5–18 cpd) could be varied between blocks of trials and the patterns expanded with temporal frequencies (TF) of 0–24 Hz. Stimuli were presented within circular apertures: *central* stimuli had inner and outer diameters of 0.5° and 5°, respectively (Fig. 1A–C); *peripheral* stimuli had inner and outer diameters of 5° and 7° (Fig. 1D–F). These
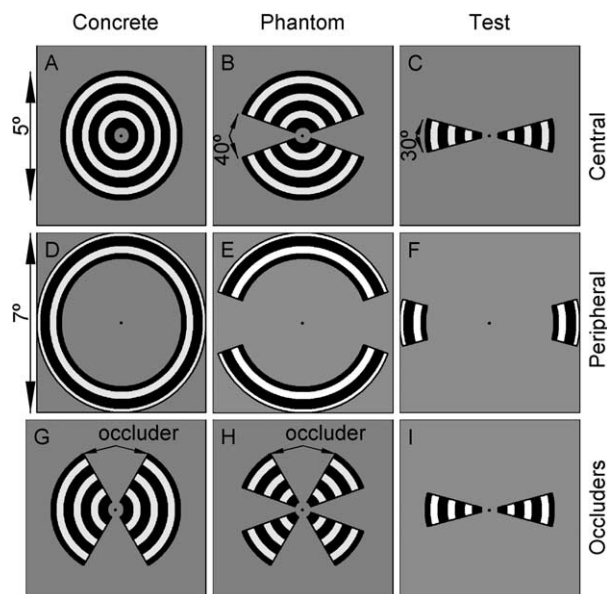

Fig. 1. Expanding concentric ring stimuli used for adapting (columns 1 and 2) and testing the MAE (column 3). Stimuli were presented centrally (top row; 0.5°–5° diameter) and peripherally (middle row; 5°–7° diameter), with adapting stimuli described as concrete if they comprised a full annulus. Phantom stimuli had two horizontal sectors of 40° arc set to the mean background luminance. Test stimuli comprised two horizontal sectors of 30° arc. In addition, we used occluding sectors of 0°–140° arc to mask regions of the adapting stimulus (G, H).

sizes were chosen so that central and peripheral stimuli covered the same area of the visual field. The screen background was maintained at the mean luminance of 33.5 cd/m^2.

Two types of adapting stimuli were used to generate MAEs: *concrete adaptors* used the full annulus (Fig. 1A and D); *phantom adaptors* were identical except for two horizontal sectors of 40° arc set to the mean luminance (Fig. 1B and E). Importantly, no illusory contours were seen by any subjects in the test region during phantom adaptation. For both adaptors, MAEs were tested in two horizontal sectors of 30° arc, such that the phantom adaptor and test regions did not abut (Fig. 1C and F). The test stimuli had the same SF and contrast as the adapting stimuli. We refer to the "adapting arc" as the effective circumference of the adapting stimulus. Thus the concrete adaptor has an adapting arc of 360°, while the two blank 40° sectors in the phantom adaptor reduce its adapting arc to 280° (Fig. 1B). To assess the impact of the adapting area on the MAEs, we used occluding vertical sectors of variable size to set patches of the adapting stimulus to the background luminance (Fig. 1G–I). With concrete stimuli we used adapting arcs of 40°–360° while phantom stimuli had adapting arcs of 80°–280°.

2.2. Procedure

Subjects viewed the screen binocularly at a distance of 1800 mm for spatial frequencies of 1.5–6 cpd or 3000 mm for higher spatial frequencies (12–18 cpd). A central red spot was provided to aid fixation. Each block of trials comprised an initial adaptation period of 30 s followed by 32 test periods (0.4 s duration) alternating with 5 s of top-up adaptation. We used motion nulling to quantify the strength of the motion aftereffect. After each test period, the screen went blank and the subject indicated the perceived direction of motion (expansion or contraction) by a button press. The adapt and test stimuli had the same spatial frequency, while the test temporal frequency was varied according to the method of constant stimuli, typically between values of −0.5 Hz (contracting) and 1 Hz (expanding). Each adaptation condition was tested with at least two blocks of trials. In total, there were over 200 blocks of trials run on each subject with a minimum of 10 minutes break between blocks.

In pilot studies, we attempted to quantify motion adaptation by measuring MAE durations. While concrete MAEs could be measured, phantom MAEs were highly variable in duration or were not perceived at all. Even with low contrast test patterns, the stationary test pattern completely removed the perception of the phantom MAE. Similarly, Bex et al. (1999) quantified the duration of concrete, but not phantom MAEs. These findings contrast the results of Hershenson (Hershenson, 1984), who was able to time phantom MAEs produced in the lower half of a spiral stimulus after adaptation to the upper half of the spiral.

2.3. Analysis

The three authors were the primary subjects in the experiments. In addition, three naïve subjects were tested with a small sample of conditions to assess the effects of varying stimulus size. For each adapting condition, logistic functions (1) were fitted to the data and confidence intervals found using 999 simulations of a bootstrap method implemented by *psignifit* (Wichmann & Hill, 2001a, 2001b).

$$P_{exp} = 1/(1 + \exp(-(TF - PSE)/\beta)) \tag{1}$$

P_{exp} is the probability that the subject sees a stimulus with temporal frequency 'TF' as expanding. PSE is the point of subjective equality; β controls the slope.

From these fits, the motion aftereffect strength was quantified as the point of subjective equality (PSE), which represents the test TF perceived as being stationary, i.e. test TFs greater than the PSE were typically seen as expanding while lower TFs were seen as contracting. Larger PSEs correspond to stronger motion adaptation and a stronger MAE. Control trials with a stationary adapting pattern always had PSEs that were zero or negative.

Data points and the corresponding response probability curves for one subject adapted to phantom and concrete stimuli at 3 cpd, 4 Hz are shown (Fig. 2). Errorbars show the positive and negative bounds of the 68% confidence limit on the PSE, as calculated from the bootstrapping process. These confidence limits approximate ±1 standard deviation from the mean for a
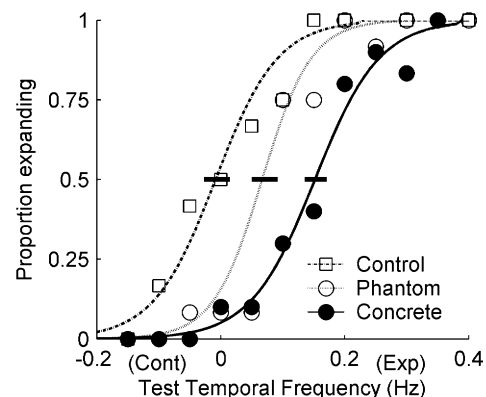

Fig. 2. Response probability curves for subject NP. The control curve (□) was measured after viewing a stationary 3 cpd concentric ring stimulus. Phantom (O) and concrete (●) results were measured after adaptation by the same ring stimulus expanding at 4 Hz. Curves represent the best fit logistic curve. Errorbars show ±1 SD in the point of subjective equality (PSE).

Gaussian distribution and for simplicity will be referred to as the standard deviation. A Monte Carlo technique implemented by *pfcmp* (Wichmann & Hill, 2001a, 2001b) showed that the PSEs produced by each adaptation condition are significantly different from the control condition (Concrete: $p < 0.01$, Phantom: $p = 0.068$).

In the subsequent results, unless otherwise stated, values are expressed relative to a stationary control: the PSE shift measured with a 0 Hz adapting pattern. Since these control conditions often produced significantly negative PSE shifts, indicating a natural bias toward expansion, this relative shift gives a measure of the strength of motion adaptation in overcoming pre-existing biases.

2.4. Eye Movements

The eye movements of two subjects (NP, MI) were monitored while performing a sample of the experiments. The lateral and vertical positions of one eye were sampled at 1 kHz using a magnetic scleral search coil (CNC Engineering, Seattle, WA). For subject NP, during the initial 30 s adaptation period, the actual point of fixation was within 0.18° of the fixation spot 75% of the time and within 0.27° for 95% of the time. For subject MI, the 75% and 95% bounds were 0.39° and 0.91°. For comparison, the equivalent positional boundaries when fixating an isolated red spot were: 0.12° and 0.15° (NP); 0.15° and 0.44° (MI). Thus the actual point of fixation was over the central gray region at least 75% of the time.

3. Results

3.1. Spatiotemporal tuning of the MAE

Subjects were presented with moving radial gratings with a range of temporal (0–24 Hz) and spatial (1.5–18 cpd) frequencies. The spatial and temporal frequencies in each set of trials were randomly interleaved. The data in Figs. 3 and 4 show PSE magnitude for concrete and phantom stimuli as a function of adapting temporal frequency (left column) or adapting velocity (right column: velocity = TF/SF).

The raw data for concrete stimuli are shown for subject NP (Fig. 3, top row). Each point is plotted relative to the 0 Hz control tested with the same SF. For ease of comparison, the raw data is also shown normalised relative to the peak response for each SF (second row). This allows direct comparison of the peak in each TF-tuning plot. It is evident that the peak PSE shift occurs in the same range (8–16 Hz) for spatial frequencies 1.5–12 cpd (Fig. 3C). At 18 cpd, the peak PSE shift occurs at the lower TF of 4 Hz. The systematic shift of the peak responses to lower temporal frequencies with
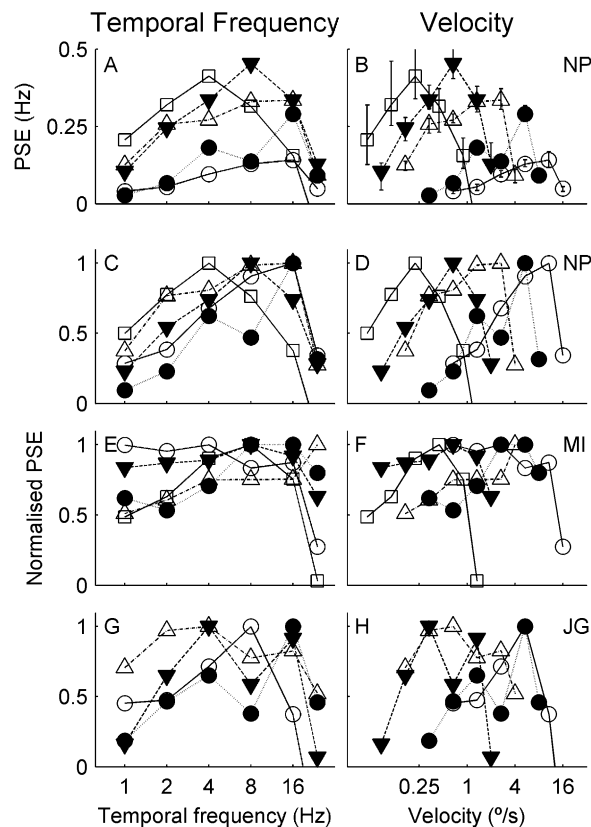

Fig. 3. Spatiotemporal frequency tuning of concrete adaptation. Raw data for subject NP is shown plotted as a function of temporal frequency (A) and velocity (B). The same data is plotted normalised relative to the peak response at each spatial frequency (C, D). Normalised data is shown for two other subjects. Errorbars (±1 SD) for MI and JG are similar to those for NP but are omitted for clarity. The peak and standard deviation of the PSE shifts at each spatial frequency were: NP: 1.5 cpd–0.14 (0.03) Hz, 3 cpd–0.29 (0.03) Hz; 6 cpd–0.34 (0.04) Hz; 12 cpd–0.45 (0.08) Hz, 18 cpd–0.41 (0.1) Hz. MI: 1.5 cpd–0.07 (0.004) Hz; 3 cpd–0.12 (0.01) Hz; 6 cpd–0.15 (0.02) Hz; 12 cpd–0.29 (0.04); 18 cpd–0.39 (0.05) Hz. JG: 1.5 cpd–0.09 (0.02) Hz; 3 cpd–0.20 (0.03) Hz; 6 cpd–0.33 (0.03) Hz; 12 cpd–0.48 (0.05) Hz. Markers for each spatial frequency are: 1.5 cpd ○; 3 cpd ●; 6 cpd △; 9 cpd ▼; 18 cpd □.

increasing spatial frequency is strong counter-evidence for speed tuning. However, the narrow band of TFs which produce peak PSE shifts is suggestive of temporal frequency tuning of the concrete MAE. Similar indications of temporal frequency tuning were obtained in two other subjects with the peak responses occurring at 8–16 Hz for MI and 4–16 Hz for JG. However, the bandpass nature of the responses at each spatial frequency is not as clear as for subject NP.

The normalised PSE shifts associated with phantom MAEs produced by adapting stimuli with spatial frequencies 1.5–12 cpd are shown in Fig. 4. Again, raw data are shown for only one subject, with normalised responses shown for all subjects. Subject NP showed alignment of the maximal PSEs at approximately the same speed (1–2°/s) irrespective of the spatial frequency
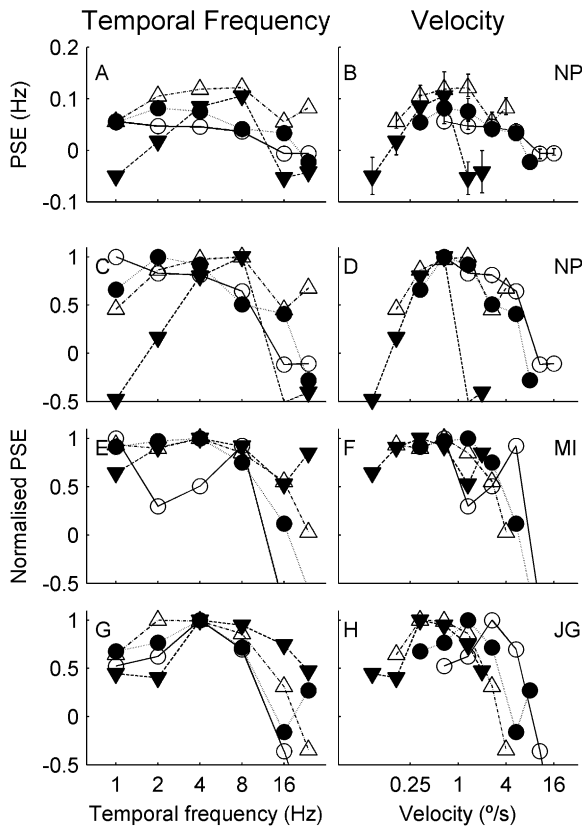
Fig. 4. Spatiotemporal frequency tuning of phantom adaptation. Raw data is shown only for subject NP, normalised data is shown for three subjects. The peak and standard deviation of the PSE shifts at each spatial frequency were: NP: 1.5 cpd–0.06 (0.01) Hz; 3 cpd–0.08 (0.02) Hz; 6 cpd–0.12 (0.03) Hz; 12 cpd–0.11 (0.03) Hz. MI: 1.5 cpd–0.04 (0.01) Hz; 3 cpd–0.08 (0.02) Hz; 6 cpd–0.11 (0.01) Hz; 12 cpd–0.16 (0.03) Hz. JG: 1.5 cpd–0.07 (0.02) Hz; 3 cpd–0.11 (0.02) Hz; 6 cpd–0.10 (0.02) Hz; 12 cpd–0.32 (0.04) Hz. Markers for each spatial frequency are the same as in Fig. 3: 1.5 cpd ○; 3 cpd ●; 6 cpd △; 9 cpd ▼; 18 cpd □.

(Fig. 4B and D). This velocity tuning was not observed in Subject JG, who showed peak PSEs at temporal frequencies 2–4 Hz irrespective of SF (Fig. 4G). Subject MI showed intermediate tuning, with similar responses to a range of temporal frequencies at each spatial frequency (Fig. 4E and F). This broad tuning is not suggestive of velocity or temporal frequency tuning.

A consistent observation across subjects and adaptation types was that higher spatial frequencies produced much larger PSEs when measured as a nulling temporal frequency. If PSE strength were presented as a nulling velocity rather than a nulling temporal frequency, there is a weaker, but consistent reversal in the relationship: the PSE measured as a nulling velocity decreases as spatial frequency is increased.

No systematic differences in response variability were found between responses to concrete and phantom stimuli, despite the PSEs produced by concrete stimuli being, on average, twice those produced by phantom stimuli. The coefficient of variation averaged across all spatial and temporal frequencies tested and all subjects

was $14 \pm 6\%$ for concrete stimuli and $20 \pm 5\%$ for phantom stimuli, suggesting that the error in the PSE increases systematically with response size. Therefore the difficulty in assigning temporal frequency or velocity tuning to responses associated with phantom adaptation cannot simply be attributed to a higher response variability. In conclusion, while the concrete MAEs show clear temporal frequency tuning, the phantom MAEs reveal a less well defined tuning mechanism.

3.2. Dependence of the MAE on eccentricity

We tested MAEs in central and more peripheral locations of the visual field using a 6 cpd grating with a range of adapting temporal frequencies. The total area of the visual field stimulated in the two positions was the same. Fig. 5 shows the PSEs generated by concrete and phantom stimuli (left and right columns, respectively) in central (○) and peripheral (△) locations. In all cases, concrete stimuli produced much greater PSE shifts than the corresponding phantom stimuli. For all subjects and all temporal frequencies, concrete stimulation in peripheral locations produced PSE shifts approximately twice as large as central locations. The same trends were observed with phantom stimulation except for subject JG tested with 1–2 Hz stimuli.

3.3. Dependence of the MAE on stimulus arc

In Fig. 6 we show the effect of altering the adapting stimulus size on the motion aftereffect. Stimulus size is represented by the total arc subtended by the adapting stimulus, which varied from $40°$ to $360°$ for concrete
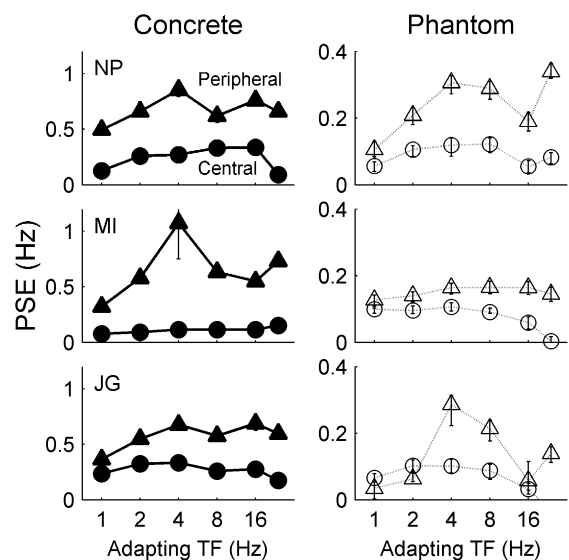

Fig. 5. Effect of eccentricity on MAE. Results are shown for three subjects tested with peripheral (▲, △) and central (●, ○) stimuli under concrete (left) and phantom (right) adapting conditions. Adapting stimuli had spatial frequency 6 cpd and temporal frequency 1–24 Hz.
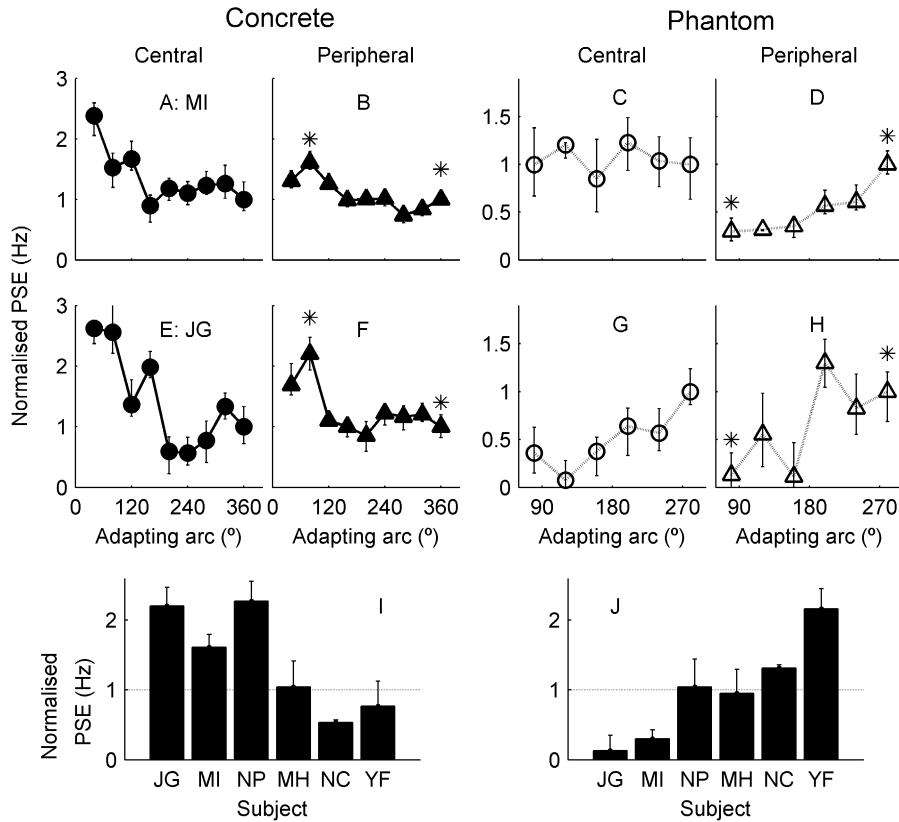
Fig. 6. Effect of adapting arc on MAE. PSEs associated with concrete and phantom stimulation in central and peripheral locations. Errorbars show ±1 SD. Results have been normalised relative to the PSE shift with the largest adapting arc (360° for concrete, 280° for phantom).

stimuli and 80°–280° for phantom stimuli. Results are shown for central and peripheral locations and have been normalised relative to the PSE shift measured with the largest adapting arc (360°—concrete; 280°—phantom). Results for the full range of stimulus sizes, positions and adaptation conditions are shown for subjects MI (A–D) and JG (E–H).

For concrete tests, the largest adaptation occurred when the adapting stimuli were smallest (40°–80° arc). In this case, the adapting stimulus approximated two isolated, translating gratings with opposite directions of motion. For phantom tests, the opposite trends were observed: the largest PSE shifts were produced by the largest stimuli.

Based on the larger PSE shifts found with peripheral adaptation, we tested a further four subjects with two stimulus sizes presented only in the periphery. For the concrete condition, the stimulus arcs were 80° and 360°; for the phantom condition, stimulus arcs were 80° and 280°. These stimulus sizes are indicated by (*) in Fig. 6. The bar charts in Fig. 6 show the shifts associated with the smaller stimulus, normalised relative to the PSE shift caused by the large stimulus. This is the same method of analysis as used for the plots at the top of Fig. 6. Values close to 1 indicate that changing stimulus size did not affect the PSE. Values greater than one indicate that

smaller stimulus arcs increase the PSE. Clearly subjects are differently affected by stimulus size. One subject (MH) showed no modulation in PSE shift with changing stimulus size. Another subject showed modulation in PSE shifts associated with changing the size of a concrete stimulus, but no effects when phantom stimulus size was changed (NP).

However, in the four of six subjects who showed significant effects of stimulus arc it is apparent that concrete and phantom stimuli produce opposite shift directions. In two subjects (MI, JG), a reduction in stimulus arc produced larger PSE shifts for concrete stimulation, while smaller PSE shifts were produced for phantom stimulation. In contrast, for two other subjects (NC, YF), reducing stimulus arc produced smaller PSE shifts for concrete stimulation, but larger PSE shifts for phantom stimulation.

3.4. Are we permanently adapted to expansion?

A surprising finding was that all subjects showed negative PSE shifts in the control condition. Thus, when the adapting pattern was stationary, subjects were biased towards indicating that the test patterns were expanding. In pilot testing, we tested subjects with a blank adapting pattern and found a similar,
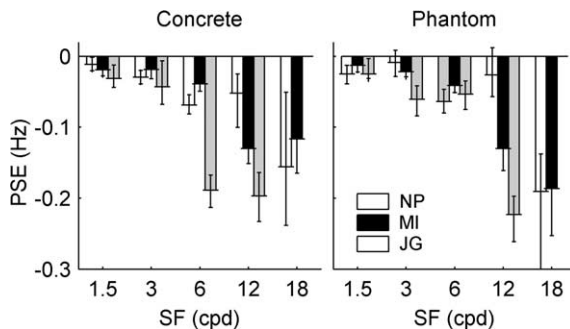
Fig. 7. PSE shifts in three subjects measured after adapting to stationary rings with SF 1.5–18 cpd. Note that the ordinate values are negative, thus they correspond to perceived expansion.

but stronger, bias. The stationary adapting pattern was thus introduced in an attempt to reduce this bias. Fig. 7 shows the PSE shifts for the stationary control conditions tested across a range of spatial frequencies. The same trends were observed for concrete and phantom conditions. In addition to the strong shifts in the control condition, the spatial frequency dependence of the shift matches that seen in the spatio-temporal frequency tuning plots shown in Fig. 3. Thus, larger shifts were observed at higher spatial frequencies.

4. Discussion

We used phantom and concrete motion aftereffects generated by radially expanding gratings to study the interactions of local and global motion detectors. We studied the velocity and spatiotemporal frequency tuning for radial gratings, which have previously only been studied using translating gratings. Similarly, our study is the first analysis of the effects of stimulus size and eccentricity on the strength of phantom MAEs generated by radial stimuli.

4.1. Spatiotemporal frequency and velocity tuning

Our results for concrete MAEs show a strong temporal frequency dependence, with maximal PSE shifts occurring with adapting stimuli of 8–16 Hz across the spatial frequencies 1.5–12 cpd. This frequency range is similar to that observed with translating and rotating gratings (Pantle, 1974; Wright & Johnston, 1985) and matches the preferred temporal frequency of human V1 and V5 as measured with fMRI (Singh, Smith, & Greenlee, 2000). This suggests that similar, local motion processors may generate the perceptual effects associated with concrete MAEs produced by translation and expansion.

Concrete MAEs showed a strong spatial frequency dependence, with increasing spatial frequency producing higher PSE shifts. Wright and Johnston (1985) showed that the PSE shift associated with the MAE produced by a translating grating increases linearly with the grating's spatial frequency. Thus when they also expressed these PSE shifts as nulling velocities, by taking the quotient of the PSE (in Hz) and the grating's SF, they found that PSEs were almost constant, regardless of spatial frequency. While we showed that increasing the stimulus spatial frequency increased the PSE (expressed as nulling temporal frequency), we did not find the same constancy when PSEs were expressed as nulling velocities. Rather, we found that nulling velocity decreased as spatial frequency increased.

Phantom MAEs did not show the same clear temporal frequency tuning as concrete MAEs. One subject had clear TF tuning (JG), one showed intermediate tuning that was neither TF nor velocity (MI) and the third showed velocity tuning (NP). This suggests that the locus for the phantom MAE does not have clear velocity or temporal frequency tuning.

In non-human primates, direction-selective neurons in the primary visual cortex (V1) are tuned to specific spatial and temporal frequencies rather than to speed (Foster et al., 1985). In contrast, speed tuning is common in direction-selective neurons in the middle temporal area (Perrone & Thiele, 2001, 2002; Rodman & Albright, 1987). Perrone and Thiele (2002) suggest that speed tuning in area MT may arise by recruiting the outputs from V1 neurons with different combinations of peak spatial and temporal tuning. Recently however, Priebe et al. have argued that only 25% of area MT neurons show true velocity tuning when tested with single sine-wave gratings (Priebe et al., 2003). They found a continuum in the degree to which preferred speed is spatial frequency dependent. Thus, it is likely that cells in area MT provide speed and temporal-frequency dependent inputs to MST neurons, which have more global receptive fields. If a similar situation is evident in human cortex, it would be difficult to categorically identify speed or TF tuned mechanisms using psychophysical tests that attempt to isolate the responses of area MT or MST.

Our psychophysical results demonstrate temporal frequency tuning of concrete MAEs, consistent with the adaptation of local motion detectors in V1, which are temporal frequency tuned. Phantom MAEs showed speed tuning in one subject and TF tuning in others, consistent with the continuum of SF dependent responses in areas MT and MST. However, further work is necessary to prove the hypothesis that adaptation of optic flow sensitive neurons in area MT or MST facilitates the phantom MAE.

4.2. Stimulus eccentricity

We showed that the strength of the motion aftereffect produced by expanding rings increased when we presented the stimulus in a more peripheral location. While this may be an effect of stimulus shape or the multiple stimulus boundaries present in the peripheral stimulus, previous studies using translating gratings in isolated and centre-surround configurations have demonstrated that MAE strength scales with eccentricity (Murakami & Shimojo, 1995; Wright, 1986). Wright and Johnston (1985) also showed that the nulling *velocity* of the MAE increases with eccentricity, in a manner approximating M-scaling in the cortex. These eccentricity-dependent changes in MAE have been attributed to spatial inhomogeneities across the visual field, such as variations in receptive field size and spatial frequency tuning.

Our results demonstrate that this spatial inhomogeneity also affects the MAE associated with complex motion. This higher sensitivity to expansion in the periphery may simply reflect that optic flow is more salient in the periphery. For example, if the speed of locomotion is changed, the changes in local velocity at any point in the visual field are much greater in the periphery than at the fovea. Thus it may be more reliable to analyse optic flow in the periphery and effectively ignore or scale down foveal optic flow. Despite this, foveal optic flow is still important for calculating heading direction.

4.3. Response summation and local inhibition

We found that phantom and concrete MAEs show different size-dependencies in different subjects. In four of six subjects showing significant size-dependent modulation of PSE shift, two subjects showed increasing phantom MAE strength and decreasing concrete MAE strength as stimulus size was increased. Two subjects showed the opposite trend.

The opposing nature of these results suggests that subjects may use different response strategies when presented with different stimulus sizes. Below, we discuss two physiological phenomena that may affect the size-dependence of the MAE. Given the variability in the response types, it is likely that there is a continuum of response strategies between these two phenomena, rather than a winner-take-all scenario. The variability in responses may also reflect the different nature of the stimuli at small and large stimulus sizes. When the adapting stimulus has a large arc it represents true expansion. As the adapting arc is reduced, the stimulus simply becomes two translating gratings with opposed motion directions. This may give different cues to the subjects. Since small test stimuli were necessary to characterise the phantom MAE, it is also possible that they predisposed the MAE measurements to those associated

with adaptation of translation-sensitive rather than expansion-sensitive cells. Further, for the peripheral stimuli, there was no motion presented around the focus of expansion, which may suboptimally stimulate an expansion detector.

We hypothesise that the phantom MAE could arise from adaptation of cells sensitive to expansion. Stimuli adapting only part of the cell's receptive field could lead to an MAE expressed in another part of the receptive field. Since physiological responses in area MST scale with stimulus size (Eifuku & Wurtz, 1998), we may expect that as stimulus size increases, the MAE strength shows a corresponding increase. This could account for the increasing PSE shift observed with increasing stimulus arc.

Centre-surround interactions in direction-selective neurons may account for the reduction in PSE shift as stimulus size is increased. Direction-selective neurons often have inhibitory surrounds (Allman, Miezin, & McGuinness, 1985a, 1985b) and there is psychophysical evidence that contextual information and relative motion affect the motion aftereffect (Murakami & Shimojo, 1995; Wade et al., 1996). Further, a decrease in MAE with increasing stimulus size has been reported for high contrast stimuli (Sachtler & Zaidi, 1993; Tadin, Lappin, Gilroy, & Blake, 2003). Since the size of our MAE test stimulus may predispose us to testing the adaptation of a translation-sensitive unit in area V1 or MT, it is possible that increasing the arc subtended by the concentric ring stimulus would reduce the response in translation-sensitive cells with inhibitory surrounds. Thus increasing the size of the motion stimulus would actually reduce its potency.

4.4. Permanent adaptation to expansion?

The anomalous motion illusion in which subjects are biased to indicate a stationary test stimulus as expanding is surprising. It may arise to counteract long-term adaptation associated with locomotion, however, the control stimuli were perceived as expanding even when the subject was tested after remaining stationary for over two hours. Thus it may reflect an innate bias in motion detection as described previously (Edwards & Badcock, 1993; Georgeson & Harris, 1978). Our finding also raises the question of why we do not perceive the world as contracting whenever we stop walking. It has been argued that vestibular input may override any visual motion adaptation (Harris, Morgan, & Still, 1981), however, the use of visual context is an alternative explanation. Wade has suggested that the MAE arises only if there is differential adaptation of restricted retinal regions (Wade & Salvano-Pardieu, 1998; Wade et al., 1996). Further, using centre-surround stimuli it has been demonstrated that the strength of a motion aftereffect in

a particular retinal location is increased if it is surrounded by a stationary stimulus and further increased if surrounded by a stimulus moving in the opposite direction (Murakami & Shimojo, 1995). Thus whole-field motion associated with locomotion may not generate an MAE because the whole retinal field is uniformly adapted.

References

Allman, J., Miezin, F., & McGuinness, E. (1985a). Direction-and velocity-specific responses from beyond the classical receptive field in the middle temporal visual area (MT). *Perception, 14*(2), 105–126.

Allman, J., Miezin, F., & McGuinness, E. (1985b). Stimulus specific responses from beyond the classical receptive field: neurophysiological mechanisms for local-global comparisons in visual neurons. *Annual Review of Neuroscience, 8*, 407–430.

Bex, P. J., Metha, A. B., & Makous, W. (1999). Enhanced motion aftereffect for complex motion. *Vision Research, 39*, 2229–2238.

Bonnet, C., & Pouthas, V. (1972). Interactions between spatial and kinetic dimensions in movement aftereffect. *Perception and Psychophysics, 12*, 193–200.

Cavanaugh, J. R., Bair, W., & Movshon, J. A. (2002). Nature and interaction of signals from the receptive field center and surround in macaque V1 neurons. *Journal of Neurophysiology, 88*(5), 2530–2546.

Duffy, C. J., & Wurtz, R. H. (1991). Sensitivity of MST neurons to optic flow stimuli. I. A continuum of response selectivity to large-field stimuli. *Journal of Neurophysiology, 65*(6), 1329–1345.

Edwards, M., & Badcock, D. R. (1993). Asymmetries in the sensitivity to motion in depth: a centripetal bias. *Perception, 22*(9), 1013–1023.

Eifuku, S., & Wurtz, R. H. (1998). Response to motion in extrastriate area MSTl: center-surround interactions. *Journal of Neurophysiology, 80*(1), 282–296.

Foster, K. H., Gaska, J. P., Nagler, M., & Pollen, D. A. (1985). Spatial and temporal frequency selectivity of neurones in visual cortical areas V1 and V2 of the macaque monkey. *Journal of Physiology, 365*, 331–363.

Georgeson, M. A., & Harris, M. G. (1978). Apparent foveofugal drift of counterphase gratings. *Perception, 7*(5), 527–536.

Harris, L. R., Morgan, M. J., & Still, A. W. (1981). Moving and the motion after-effect. *Nature, 293*(5828), 139–141.

Hershenson, M. (1984). Phantom spiral aftereffect: evidence for global mechanisms in perception. *Bulletin of the Psychonomic Society, 22*(6), 535–537.

Murakami, I., & Shimojo, S. (1995). Modulation of motion aftereffect by surround motion and its dependence on stimulus size and eccentricity. *Vision Research, 35*(13), 1835–1844.

Nawrot, M., & Sekuler, R. (1990). Assimilation and contrast in motion perception: explorations in cooperativity. *Vision Research, 30*(10), 1439–1451.

Pantle, A. (1974). Motion aftereffect magnitude as a measure of the spatio-temporal response properties of direction-sensitive analyzers. *Vision Research, 14*, 1229–1236.

Perrone, J. A., & Thiele, A. (2001). Speed skills: measuring the visual speed analyzing properties of primate MT neurons. *National Neuroscience, 4*(5), 526–532.

Perrone, J. A., & Thiele, A. (2002). A model of speed tuning in MT neurons. *Vision Research, 42*(8), 1035–1051.

Priebe, N. J., Cassanello, C. R., & Lisberger, S. G. (2003). The neural representation of speed in macaque area MT/V5. *Journal of Neuroscience, 23*(13), 5650–5661.

Rodman, H. R., & Albright, T. D. (1987). Coding of visual stimulus velocity in area MT of the macaque. *Vision Research, 27*(12), 2035–2048.

Sachtler, W. L., & Zaidi, Q. (1993). Effect of spatial configuration on motion aftereffects. *Journal of Optical Society of America A, 10*(7), 1433–1449.

Singh, K. D., Smith, A. T., & Greenlee, M. W. (2000). Spatiotemporal frequency and direction sensitivities of human visual areas measured using fMRI. *Neuroimage, 12*(5), 550–564.

Snowden, R. J., & Milne, A. B. (1997). Phantom motion aftereffects—Evidence of detectors for the analysis of optic flow. *Current Biology, 7*(10), 717–722.

Tadin, D., Lappin, J. S., Gilroy, L. A., & Blake, R. (2003). Perceptual consequences of centre-surround antagonism in visual motion processing. *Nature, 424*(6946), 312–315.

Tanaka, K., Hikosaka, K., Saito, H., Yukie, M., Fukada, Y., & Iwai, E. (1986). Analysis of local and wide-field movements in the superior temporal visual areas of the macaque monkey. *Journal of Neuroscience, 6*(1), 134–144.

von der Heydt, R., Peterhans, E., & Baumgartner, G. (1984). Illusory contours and cortical neuron responses. *Science, 224*(4654), 1260–1262.

von Grunau, M. W. (1986). A motion aftereffect for long-range stroboscopic apparent motion. *Perception and Psychophysics, 40*(1), 31–38.

von Grunau, M. W., & Dube, S. (1992). Comparing local and remote motion aftereffects. *Spatial Vision, 6*(4), 303–314.

Wade, N. J. (1994). A selective history of the study of visual motion aftereffects. *Perception, 23*(10), 1111–1134.

Wade, N. J., & Salvano-Pardieu, V. (1998). Visual motion aftereffects: differential adaptation and test stimulation. *Vision Research, 38*(4), 573–578.

Wade, N. J., Spillmann, L., & Swanston, M. T. (1996). Visual motion aftereffects: critical adaptation and test conditions. *Vision Research, 36*(14), 2167–2175.

Weisstein, N., Maguire, W., & Berbaum, K. (1977). A phantom-motion aftereffect. *Science, 198*, 955–958.

Wichmann, F. A., & Hill, N. J. (2001a). The psychometric function: I. Fitting, sampling, and goodness of fit. *Perception and Psychophysics, 63*(8), 1293–1313.

Wichmann, F. A., & Hill, N. J. (2001b). The psychometric function: II. Bootstrap-based confidence intervals and sampling. *Perception and Psychophysics, 63*(8), 1314–1329.

Wright, M. J. (1986). Apparent velocity of motion aftereffects in central and peripheral vision. *Perception, 15*(5), 603–612.

Wright, M. J., & Johnston, A. (1985). Invariant tuning of motion aftereffect. *Vision Research, 25*(12), 1947–1955.

Zaidi, Q., & Sachtler, W. L. (1991). Motion adaptation from surrounding stimuli. *Perception, 20*, 703–714.